

Research on the Influencing Rules of Gas Hydrate Emission Dissipation Coefficient Based on Subspace Spectrum Clustering

Geng Guo^{1,*}, Leiwen Chen¹, Ji Li², Shu Yan³, Wenxiang Wu⁴, Lingxu Li⁵ and Hongda Li⁶

¹School of Economics & Management, Fuzhou University, Fuzhou, 350116, China

²School of Petroleum Engineering, Northeast Petroleum University, Daqing, 163318, China

³School of Earth Sciences, Northeast Petroleum University, Daqing, 163318, China

⁴School of Petroleum Engineering, Northeast Petroleum University, Daqing, 163318, China

⁵Third Oil Production Plant of Daqing Oilfield Co., Ltd., Daqing, 163300, China

⁶School of Petroleum Engineering, Northeast Petroleum University, Daqing, 163318, China

*Corresponding Author: Geng Guo. Email: jdjiandu@163.com

Received: 08 March 2020; Accepted: 17 April 2020

Abstract: Featured by high energy density, low combustion pollution and large quantity, natural gas hydrate has become one of the research hotspots in Sanlutian Field of Muri Coalfield since 2008, when China first drilled natural gas hydrate samples in the permafrost area of Qilian Mountains, Qinghai-Tibet Plateau. However, the study on the controlling factors of gas hydrate accumulation is still shallow, which hinders the exploration and development of natural gas hydrate resources. The controlling factors of gas hydrate accumulation mainly include temperature and pressure conditions, gas source conditions, sedimentary conditions and structural conditions, among which structural conditions are the important one. In this paper, the Sanlutian Field of Muri Coalfield in the southern margin of Qilian Mountains is selected as the main research area and natural gas hydrate is taken as the research subject. According to the sample test results, the geological structure pattern is inferred, and the occurrence characteristics, gas source and hydrate composition of Sanlutian gas hydrate samples are further obtained. Finally, the gas hydrate accumulation model at the end of structure is summarized and illustrated.

Keywords: Subspace; spectral clustering; natural gas hydrate; dissipative effects; law study

1 Introduction

The gradual decrease of conventional oil and gas resources worldwide, accompanied by the constantly increasing demands on energy and intensified supply-demand pressure, keep urging the scientists to continuously seek for new alternative energies. Since China explored the first physical sample in the perpetually frozen region with medium and low latitude on Qilian Mountain in 2008, natural gas hydrate (NGH) has aroused great concerns and attentions among scientists [1]. As a kind of new natural energy and an important unconventional oil gas resource, NGH is not only an ideal substitute for conventional oil and gas resources, but also a kind of new green and clean energy with low pollution and high efficiency, thus shedding new light on the future direction in this field [2].

As indicated by a new round of evaluation works on coal resource potential that has just been completed, it can be seen that the total quantity of coal resources of Qilian Mountain region reaches 14.082 billion tons. Coal measures serve as an important carrier of comprehensive mineral resources. Besides coal seams, various kinds of mineral resources are reserved or associated in the coal measures in different forms. Gaseous energies mainly contain coalbed methane (CBM), sandstone gas and shale gas, etc., [3] and solid-



state energies mainly contain bauxite, sedimentary uranium mine and oil shale etc., as well as solid-state NGH formed under specific conditions, etc. Referring to a saying of Novak, the Russian Minister of Energy when he was having an interview on Apr. 16, 2013, “exploitation of NGH instead of shale gas can raise a revolution in the world energy market.” As the standing stock of NGH is twice the total amount of shale gas and natural gas, technologies that are more suitable for exploitation of NGH will be invented in the long run though there has been no effective exploration and exploitation yet. In view of this, the exploitation cost will consequently be reduced [4,5]. Aimed at the broadly-distributed permafrost distribution areas in China, especially the permafrost regions on Qinghai-Tibet Plateau, academic circles have attached great importance to them and believe that these regions have the geological conditions for the formation of NGH. As early as 1999, when the national special project of “a new round of big survey on territorial resources” was started in China, a series of researches have been carried out [6]. The finding of NGH in Muri coalfield, Qinghai Province has set off another round of climax in exploration and research. Ministry of Land and Resources, China Geological Survey, Science and Technology Department of Qinghai Province and China National Administration of Coal Geology, etc., all set up projects and carried out deeper researches successively [7,8].

After years of researches on permafrost regions of Qinghai-Tibet Plateau, key breakthroughs were finally made by Chinese scientific researchers in Muri region, Qilian Mountain, Qinghai Province. As the first country in the world to collect the aquo-complex samples from perpetually frozen regions, China’s discovery of aquo-complex in Muri region and the accompanied researches on all aspects have a great significance on theoretical researches [9]. Compared with NGH from sea areas and polar region tundra, NGH from medium and low latitude present different characteristics in terms of existing conditions, rules and main controlling factors, etc. Therefore, development of fundamental researches on characteristics of NGH is helpful to the development and utilization in Qinghai-Tibet Plateau regions.

2 Dissection of Typical Oil and Gas Reservoir in Active Regions of Mud Diapiric Fold

The Muri coal and gas field at the southern edge of Qilian Mountain belongs to the gas field groups at the eastern part of Yinggehai Basin, which is the largest commercial natural gas field found in this basin through exploration up to now, and its geographical position is at the northwestern part of central mud diapir structure belt in Yinggehai Basin (Fig. 1) [10]. With a water depth of 75 m, the main pay zone of this gas field is Yinggehai of Pliocene series, now over 10 exploratory wells have been drilled in Muri coalfield 2/3 at the southern edge of Qilian Mountain, through which it was explored that when the gas bearing area was 287.7 k, the geological reserves of natural gas was explored to be $1296.38 \times 10^8 \text{ m}^3$, of which pure hydrocarbon gas took $612 \times 10^8 \text{ m}^3$, this gas field was found through exploration in the 1990s and was put into exploitation in 2003, up to the end of 2011, the accumulated output of natural gas was $171.77 \times 10^8 \text{ m}^3$.

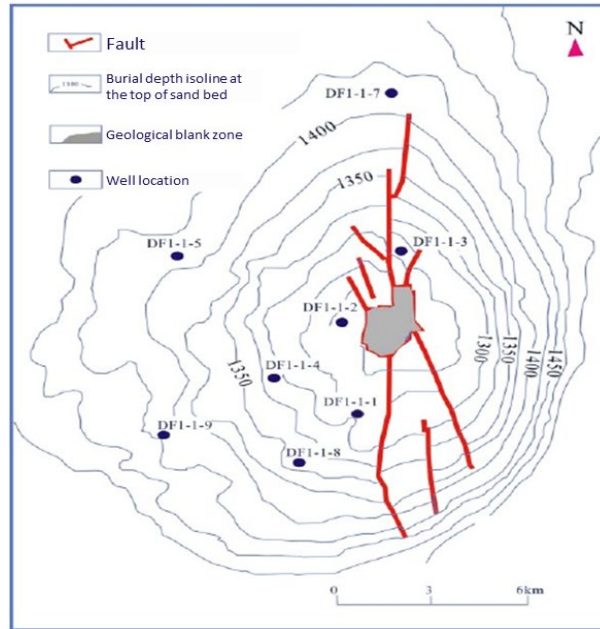


Figure 1: Fault layout and well locations of Muri coal and gas field at the southern edge of Qilian Mountain

Shallow gas reservoir of Muri coalfield at the southern edge of Qilian Mountain is located at the northwestern part of central mud diapir structure belt in Yinggehai Basin [11], whose structure is a brachyaxis anticline with inherited development that is formed through the mud diapiric fold function. Its long axis is 21 km and the minor axis is 12 km; the entrapment is of a large area, of which the area of the largest entrapment can reach 287.7 km², and it is of a high closure (closure range is 219–254.8 m) and a shallow burial, as shown in Fig. 2. The anticline structure is steep in the east and gentle in the west; a north-south breakage is developed on the tectonic axis, distributed in the shape of arborization, and the anticline structure is divided into eastern and western blocks, causing the effect that different blocks composing the wings have different pressure systems and natural gas components. Muri coal gas field at the southern edge of Qilian Mountain is a structural gas pool mainly consisting of mud diapiric fold anticlines and fault control, parts of which are lithologic gas reservoirs. The gas reservoirs contain multiple gas groups, and the distribution of gas and water is controlled by the structure and faults, which is a structural gas pool with the driving type of elastic water drive. Pressure coefficient of the gas reservoir is 1031.14, so it is a gas pool with atmospheric pressure.

The shallow gas reservoir of Muri coalfield at the southern edge of Qilian Mountain is the Yinggehai stratum of Pliocene epoch, shoals and sand bank sedimentations similar to shore-shallow sea phase belt are formed by underwater highlands deposited in the shallow sea environment, which show a high-mesoporous and low-hypotonic feature on the whole. The cap rock is the whole set marine mudstone formed by Yinggehai series and Ledong series, which is of a large thickness and good sealing feature. There are 3 types in the reservoirs of Muri coalfield at the southern edge of Qilian Mountain: the lithology of the first type is thick-bedded sandstone porous-type reservoir, which mainly consists of grey thick-layer fine sandstones, sometimes mixed with siltstone stripes, whose general thickness of single layer is 5 m. The second type is fractured argillaceous siltstone reservoir, which mainly consists of argillaceous siltstones, whose general thickness of single layer is 15 m. The lithology of the third type is argillaceous siltstone reservoir, with the reservoir space consisting of matrix micropores.

It is indicated by the geochemical characteristics of shallow gas reservoir of Muri coalfield at the southern edge of Qilian Mountain that, its source rocks are mainly from Sanya-Huangliu marine mudstone of Miocene series, the lithology of source rocks is mainly silty mudstone and mud rock, and its organic matter type is humic mixed type—humic type. The TOC content is 0.39%–0.70% with an average proportion of 0.50%, the contents of chloroform bitumen A and total hydrocarbon are respectively 0.0561%

and 353×10^{-6} , which can reach the level of good source rocks on the whole. There are great changes in the chemical constitution of natural gas in the Muri coal gas field at the southern edge of Qilian Mountain, in different air layers and even the same air layer, features of natural gas from different fault blocks and especially the contents of non-hydrocarbon gas and isotope composition of methane are widely different, and an obvious anisotropism is showed up. It can be divided into 3 types based on the content of hydrocarbon and non-hydrocarbon: the first type is the hydrocarbon gas reservoir whose natural gas component is mainly methane (over 75%), the constituent content of heavy hydrocarbon is low (3.37%), the value of aridity coefficient is 0.99, most of which is dry gas; the second type is CO₂ gas reservoir (content is as high as 5588%); and the third type is N₂—rich gas reservoir, whose Na content is as high as 1531%, and the CO₂ content is less than 5%.

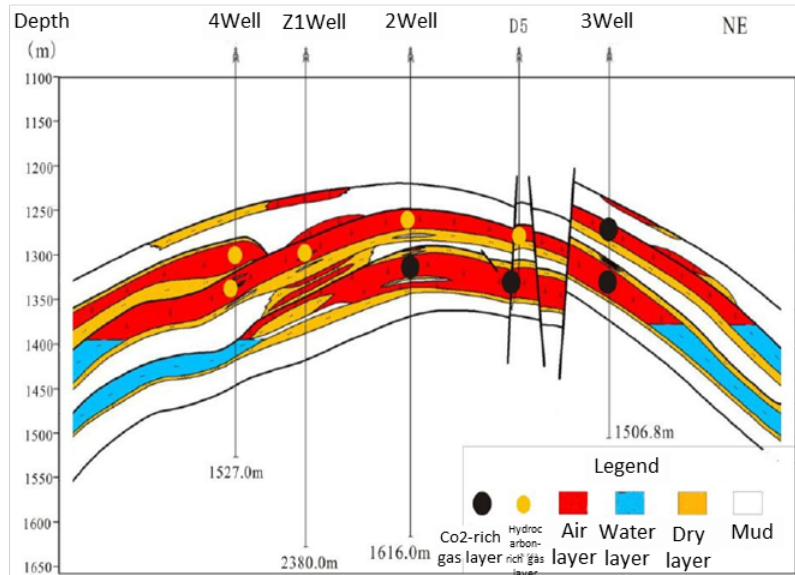


Figure 2: Profile map of gas pools of Well 4-Z1-2-DS-3 of Muri coal gas field at the southern edge of Qilian Mountain (based on materials of CNOOC)

3 Dissipation Coefficient Analysis Based on Subspace Spectral Clustering

3.1 Spectral Clustering Based on K-harmonic Mean

If dissipation coefficient analysis data is seen as a document, and the labels of dissipation coefficient analysis data are seen as the key words of the document, so if we conduct clustering with the feature of labels of dissipation coefficient analysis data, clustering of dissipation coefficient analysis data can be conducted through the method of this paper. Currently, popular clustering methods are mainly methods based on division with K-Means as representative and spectral clustering method, etc. Spectral clustering is to cluster based on graph theory and similarity among data, as it has no relationship with dimensionality of data points and simply related to the number of them, it is suitable for non-measure spaces. It has been broadly concerned, but traditional clustering algorithm is sensitive to selection of initial center, which makes its computational result unstable, and it is easy to be caught in partial minimal points. Meanwhile, there is particularity on the clustering problems of this paper, vectors of this paper are generally sparse vectors containing multiple 0, which has brought about difficulties to the selection of clustering center. Thus, the performance of spectral clustering algorithm is improved through introduction of K-harmonic means. K-harmonic means (KHM) algorithm [11] is a kind of clustering algorithm based on the center, through calculating the harmonic mean of distance from data points to the clustering center, its performance function is constructed through this algorithm. Expression of the algorithm is as follows:

Algorithm 1: K-harmonic mean spectral clustering algorithm

Input: n data points $X = (x_1, x_2 \cdots x_n)$, the number of clusters is k

Output: category of data point sets

Step 1: construct a similar matrix $A \in R^{n \times n}$, of which $a_{ij} = \exp(-\frac{\|x_i - x_j\|^2}{2\sigma^2})$, $i \neq j$, $a_{ii} = 0$. σ is a parameter.

Step 2: construct a Laplacian matrix, $L = D^{-1/2}AD^{-1/2}$. Of which D is the diagonal matrix, and $D_{ii} = \sum_{j=1}^n a_{ij}$.

Step 3: calculate the eigenvectors $e_1, e_2 \dots e_k$ of the first k maximum eigenvalues of L and generate matrix $Z = [e_1, \dots, e_k] \in R^{n \times k}$;

Step 4: convert the row vector of matrix Z to unit vector and acquire matrix $Y = Z_{ij} / (\sum_j Z_{ij}^2)^{1/2}$.

Step 5: cluster each row of matrix Y into k categories through KHM algorithm.

As the harmonic average of distance from data points to the center of all clustering replaces the minimum distance from data points to the center of clustering in KHM algorithm, it overcomes the sensitiveness on original value.

3.2 Dissipation Coefficient Analysis Data Clustering Based on Subspace

Set that $L = \{t_1, t_2, \dots, t_m\}$ is the key words glossary used to mark the dissipation coefficient analysis data, m is the scale of the glossary, set that $T = \{(I_1, w_1), (I_2, w_2), \dots, (I_n, w_n)\}$ is the training dataset of dissipation coefficient analysis, and $w_i \in L$ is a group of annotative words of dissipation coefficient analysis data I_i . If dissipation coefficient analysis data I_i is seen as a document, then w_i can be seen as the key words of the document. For each dissipation coefficient analysis data $I_i \in T$, the vector $X_i = \{x_{i1}, x_{i2}, \dots, x_{im}\}$ of its key words is constructed. If the k^{th} key word of the glossary $t_k \in w_i$, there is $x_{ik} = 1$. Or $x_{ik} = 0$. Then eigenvectors of annotative words of dissipation coefficient analysis data in the training dataset of dissipation coefficient analysis is:

$$X = [X_1 \quad X_2 \quad \dots \quad X_n]^T \quad (1)$$

Distance between the 2 eigenvectors X_i and X_j is defined as $d(X_i, X_j)$, calculate the value of $d(X_i, X_j)$ through cosine distance. With vector X of annotative word of dissipation coefficient analysis data in the text space as feature, conduct clustering through KHM clustering algorithm and form n semantic $C_i (i = 1, 2, \dots, n)$ s. Take head-word of each category as the semantics $L^i = \{w_1^i, w_2^i, \dots, w_l^i\}$ (label for category) of such category.

3.3 Low-Level Features and Semantic Mapping Relation of Dissipation Coefficient Analysis Data

Dissipation coefficient analysis data in each semantic category are divided into different regions, and the extracted low-level feature of the divided regions is expressed with vector f . f is expressed with 24-dimension vector.

Based on the similarity relation of low-level regional features, KHM algorithm is used to cluster the similar regions of the same semantic category into the same blob once again and form $Kb_i (i = 1, 2, \dots, k)$ blobs. Through the number of optimized blobs K , internal spur of each blob is concentrated as far as possible and the distance among blobs is kept away to the largest extent. To confirm the optimal value of K , several

times of clustering are conducted through setting different K s, for different K values, the distance $d_{inter}(X_i, X_j)$ among the blobs and the internal spur $d_{intra}(X_i)$ of each blob are calculated.

Based on Davies-Bouldin index [11], Formula (2) is as follows:

$$\frac{1}{k} \sum_{i=1}^k \max_{i \neq j} \left\{ \frac{d_{intra}(X_i) + d_{intra}(X_j)}{d_{inter}(X_i, X_j)} \right\} \quad (2)$$

Acquire that the K at its minimum value should be the optimal K value, that is:

$$k = \arg \min_k \frac{1}{k} \sum_{i=1}^k \max_{i \neq j} \left\{ \frac{d_{intra}(X_i) + d_{intra}(X_j)}{d_{inter}(X_i, X_j)} \right\} \quad (3)$$

Thus k blobs are acquired in each semantic category. Those blobs inherit the semantics L^i that they are in.

Through twice clustering, training dataset of dissipation coefficient analysis T is divided into several semantic categories $C_i (i=1,2,\dots,n)$, each semantic category is expressed with the central features of the usable blobs and the key words $L^i = \{w_1^i, w_2^i, \dots, w_l^i\}$ of this category:

$$C_i = \{b_1^i, b_2^i, \dots, b_k^i; L^i\} = \{b_1^i, b_2^i, \dots, b_k^i; w_1^i, w_2^i, \dots, w_l^i\} \quad (4)$$

In any semantic category, distribution of joint probability of blob b_i and key word $w_j \in L^i$ is acquired through the following formula:

$$p(w_j^i, b_i) = \sum p(w_j^i, b_i | C_i) p(C_i) = \sum p(w_j^i | b_i, C_i) p(b_i | C_i) p(C_i) \quad (5)$$

In the formula, $p(C_i)$ is the priori probability of category C_i , $p(w_j^i | b_i, C_i)$ represents the contingent probability of key word w_j^i in category C_i , it can be acquired through Dobernoulli Model that:

$$p(w_j^i | b_i, C_i) = \frac{\mu \delta_{w_j^i, C_i} + N(w_j^i)}{\mu + |C_i|} \quad (6)$$

In the above formula, μ is the coefficient of balance; if there is annotative word w_j^i in category C_j , the value of $\delta_{w_j^i, C_i}$ is 1, or it is 0. $N(w_j^i)$ represents the time of appearance of annotative word w_j^i in category C_j , and $|C_i|$ represents the number of dissipation coefficient analysis data in category C_j .

$p(b_i | C_i)$ can be acquired through calculation of the following formula:

$$p(b_i | C_i) = \frac{|b_i|}{\sum_{l=1}^k |b_l|} \quad (7)$$

4 Empirical Analysis

It can be known from the measured data of research area (Tab. 1) that the HI scope if coal sample is 55–187 mg/g and the average value is 132.73 mg/g, and it is divided into III₂-type (three-category five-group method) kerogens based on standard of coal organic matter types, which are converted to III-type kerogens through three-category inquartation rules [12,13]. The scope of (S1 + S2) is 72.09–185.31 mg/g with the average value of 129.21 mg/g, which is divided into III₁-type (three-category five-group method) kerogens, and is converted to II-type kerogens through three-category inquartation rules. HI scope of mudstone sample is 29–476 mg/g and the average value is 213 mg/g, it is divided into II-type kerogens based on standard of continental facies source rock organic matter type; scope of D is 3.74%–41.77% with

the average value of 19.56%, which is divided into II:-type kerogens; scope of (S 1 + S2) is 0.23–15.45 mg/g with the average value of 6.58 mg/g, which is divided into III-type kerogens. IH scope of oil shale samples is 112–311 mg/g, its average value is 163 mg/g, which is divided into II:-type kerogens based on standard of continental facies source rock organic matter type; scope of D is 10.67%–26.68% with the average value of 14.79%, which is divided into II:-type kerogens; scope of (S1 + S2) is 1.98–11.41 mg/g with the average value of 4.79 mg/g, which is divided into III-type kerogens. The division results can be seen in Figs. 3 and 4.

Table 1: Measured data in the study area

Project	Type I				
	Type I (sapropel type)	Type II (Rot-Rotten mud type)	Type II2 (Rotten mud-Rot type)	Type III (saprophytic)	
Form	Saturated hydrocarbon%	60–40	< 40–30	< 30–20	< 20
	Full/fragrant (non hydrocarbon + asphaltene)%	> 3.0	3.0–1.6	< 1.6–1.0	< 1.0
	(non hydrocarbon + asphaltene)%	20–40	> 40–60	> 60–70	> 70–80
	(non hydrocarbon + asphaltene) total hydrocarbon	0.3–1.0	> 1.0–2.0	> 2.0–3.0	> 3.0–4.5
Pyrolytic parameter	HI	476 mg/g	279 mg/g	148 mg/g	29 mg/g
	Y	< 20	20–10	< 10–5.0	< 5.0
	D	41.77%	31.47%	22.58%	3.74%
	(S1 + S2)	11.41 mg/g	8.79 mg/g	4.56 mg/g	1.98 mg/g

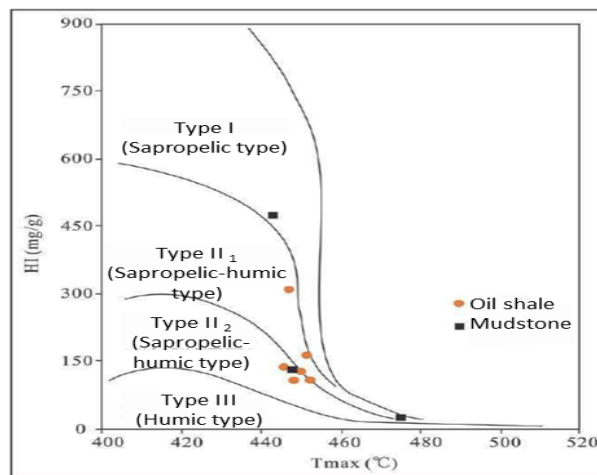


Figure 3: Tma × and HI dependency diagram of source rocks

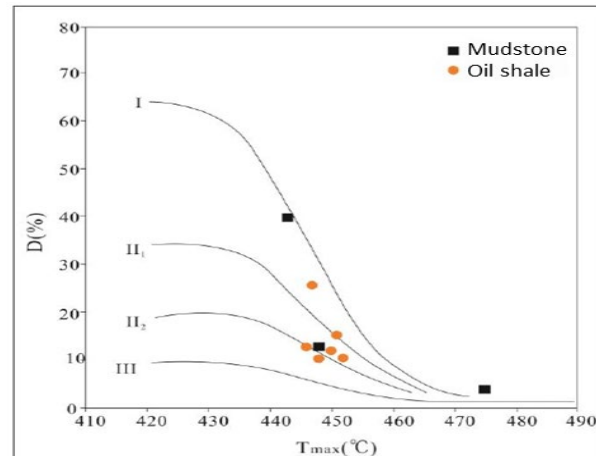


Figure 4: D-T_{max} × cultellation diagram of source rocks

Based on collection and settlement of research and experimental data of predecessors and actual measurement of samples collected from well fields and NGH drill holes of the adjacent region (measured by Emmi of national key laboratory of coal resources and safe mining), the results show that the minimum Ro value of vitrinite reflectance of coal sample is 0.71%, the maximum value is 2.26% and the average value is 1.18%. There is a little measured data of oil shale and mudstone, the Ro value of oil shale is 0.94%; the minimum Ro value of mudstone is 0.72%, the maximum value is 0.95% and the average value is 0.86%.

In addition, in the practical investigation of drill cores, oil patches can be seen many times (see Fig. 5). Thus it can be known from analysis in above text that oil shale and mudstone of the research area enter the mature stage, in which petroleum and wet gas can be generated; while coals mainly enter the mature-high-mature stage, in which petroleum, wet gas and condensate gas can be generated, individual samples show that the coals have entered the postmature stage, in which dry gas can be generated.



Figure 5: Oil patch phenomenon of drill core

5 Conclusion

It is thought through comprehensive analysis that control actions of construction on reservoir forming of NGH can be divided into 4 aspects:

(1) Structural framework controls the distribution of NGH: NGH mainly gathers in blob M₁ and S₁, etc., and it is more concentrated in areas with deeper burial depth; in addition, F₂ and F₃₀ breakage has a significant control action on its reserves.

(2) Tectonic movements control the formation of hydrocarbon gas and warm-pressing stabilized zones, in addition, it also transforms the reservoirs in 2 ways, namely deformation and deflection: main period of hydrocarbon generation of source rocks in well fields was the end of early Baiscicus, and hydrocarbon generation was stopped in later periods; formation time of perpetually frozen area of Qilian Mountain was no early than around 3.6 Ma till now, then the formation of warm-pressing stabilized zone was also no early than around 3.6 Ma till now; tectonic movements have caused permanent deformation and deflection on the reservoirs, enlarging or reducing the burial depth of gases, then it enters the warm-pressing stabilized zone and thus forming NGH reservoirs.

(3) Different structural configurations have different preserving functions on NGH: breakages and fractures provide passages for the movement of hydrocarbon gases, breakage crushed zones and fractures provide reservoir spaces beneficial for the gases, and construction formation circles store and accumulate the gases.

(4) Similar to tectonic movements, destructions of structures on NGH can be divided into transformation and deflection damages: transformation of reservoirs let off the gases and thus no NGH can be formed; deflection of reservoirs make the gases crop out and disperse, thus no NGH can be formed, or the gases are deeply buried and cannot enter the warm-pressing stabilized zones to form NGH or to be explored.

Funding Statement: Fund of Heilongjiang Province Student Innovation and Entrepreneurship Training Program Project 201910220111.

Conflicts of Interest: The authors declare that they have no conflicts of interest to report regarding the present study.

References

1. Zhao, J. F., Liu, Y. L., Guo, X. W., Wei, R. P., Yu, T. B. et al. (2020). Gas production behavior from hydrate-bearing fine natural sediments through optimized step—wise depressurization. *Applied Energy*, 260, 114275.
2. Yang, S. X., Liang, J. Q., Lu, J. A., Qu, C. W., Liu, B. (2017). New understandings on the characteristics and controlling factors of gas hydrate reservoirs in the Shenhu area on the northern slope of the South China Sea. *Earth Science Frontiers*, 24(4), 1–14.
3. Song, D. M., Liu, B., Li, X., Chen, S. C., Li, L. W. et al. (2015). Hyperspectral data spectrum and texture band selection based on the subspace-rough set method. *Remote Sensing Technology & Application*, 36(8), 16–19.
4. Xu, S. W., Amarakoon, I. D., Zaheer, R., Smith, A., Sura, S. et al. (2018). Dissipation of antimicrobial resistance genes in compost originating from cattle manure after direct oral administration or post-excretion fortification of antimicrobials. *Journal of Environmental Science & Health Part A Toxic/hazardous Substances & Environmental Engineering*, 53(4), 373–384.
5. Xie, Q., Lin, H. F., Zhang, S., Wang, R. X., Kong, F. et al. (2018). Deposition of SiC_xHyO_z thin film on epoxy resin by nanosecond pulsed APPJ for improving the surface insulating performance. *Plasma Science and Technology*, 20(2), 025504.
6. Yang, T. H., Huang, H. Y., Sun, C. C., Glorieux, B., Lee, X. H. et al. (2018). Noncontact and instant detection of phosphor temperature in phosphor-converted white LEDs. *Scientific Reports*, 8(1), 296–297.
7. Xu, R. X., Liu, Y., Zhang, H. D., Yan, Y. J. (2018). Theories of quantum dissipation and nonlinear coupling bath descriptors. *Journal of Chemical Physics*, 148(11), 114103.
8. Inampudi, S., Cheng, J., Salary, M. M., Mosallaei, H. (2018). Unidirectional thermal radiation from a SiC metasurface. *Journal of the Optical Society of America B Optical Physics*, 35(1), 39–42.
9. Kim, S., Lee, S. H., Yong, T. K. (2017). Characteristics of CO₂ hydrate formation/dissociation in H₂O + THF aqueous solution and estimation of CO₂ emission reduction by district cooling application. *Energy*, 120(6), 362–373.
10. Shakirov, R. B., Obzhairov, A. I., Salomatin, A. S., Makarov, M. M. (2017). New data on lineament control of modern centers of methane degassing in east Asian seas. *Doklady Earth Sciences*, 477(1), 1287–1290.
11. Janicki, G., Schlüter, S., Hennig, T., Deerberg, G. (2017). Numerical simulation of gas hydrate exploitation from

- subsea reservoirs in the Black Sea. *Energy Procedia*, 125(4), 467–476.
12. Frommer, A., Güttel, S., Schweitzer, M. (2014). Efficient and stable arnoldi restarts for matrix functions based on quadrature. *Siam Journal on Matrix Analysis & Applications*, 35(2), 661–683.
 13. Boriskina, S. V., Cooper, T. A., Zeng, L. P., Ni, G., Tong, J. K. et al. (2017). Losses in plasmonics: from mitigating energy dissipation to embracing loss-enabled functionalities. *Advances in Optics & Photonics*, 9(4), 775–827.